Eosinophil trafficking in allergen-mediated pulmonary inflammation relies on IL-13–driven CCL-11 and CCL-24 production by tissue fibroblasts and myeloid cells

Pedro H. Gazzinelli-Guimaraes, PhD,[a] Dominic P. Golec, PhD,[b] Erik P. Karmele, PhD,[c] Joshua Sciurba, BSc,[a] Pablo Bara-Garcia, MSc,[a] Tom Hill, PhD,[d] Byunghyun Kang, PhD,[c] Sasisekhar Bennuru, PhD,[a] Pamela L. Schwartzberg, MD,[b] and Thomas B. Nutman, MD[a] *Bethesda, Md*

Background: The immunologic mechanisms underlying pulmonary type 2 inflammation, including the dynamics of eosinophil recruitment to the lungs, still need to be elucidated.
Objective: We sought to investigate how IL-13–producing T_H2 effector cells trigger eosinophil migration in house dust mite (HDM)-driven allergic pulmonary inflammation.
Methods: Multiparameter and molecular profiling of murine lungs with HDM-induced allergy was investigated in the absence of IL-13 signaling by using IL-13Rα1–deficient mice and separately through adoptive transfer of $CD4^+$ T cells from IL-5–deficient mice into $TCR\alpha^{-/-}$ mice before allergic inflammation.
Results: We demonstrated through single-cell techniques that HDM-driven pulmonary inflammation displays a profile characterized by T_H2 effector cell–induced IL-13–dominated eosinophilic inflammation. Using HDM-sensitized IL-13Rα1$^{-/-}$ mice, we found a marked reduction in the influx of eosinophils into the lungs along with a significant downregulation of both CCL-11 and CCL-24. We further found that eosinophil trafficking to the lung relies on production of IL-13–driven CCL-11 and CCL-24 by fibroblasts and $Ly6C^+$ (so-called classical) monocytes. Moreover, this IL-13–mediated eotaxin-dependent eosinophil influx to the lung tissue required IL-5–induced eosinophilia. Finally, we demonstrated that this IL-13–driven eosinophil-dominated pulmonary inflammation was critical for limiting bystander lung transiting *Ascaris* parasites in a model of allergy and helminth interaction.
Conclusion: Our data suggest that IL-5–dependent allergen-specific T_H2 effector cell response and subsequent signaling through the IL-13/IL-13Rα1 axis in fibroblasts and myeloid cells regulate the eotaxin-dependent recruitment of eosinophils to the lungs, with multiple downstream consequences, including bystander control of lung transiting parasitic helminths. (J Allergy Clin Immunol Global 2023;2:100131.)

Key words: *Type 2 inflammation, eosinophils, allergy, asthma, IL-13 signaling, CCL-11, CCL-24, T_H2 cell response, helminth parasites*

Type 2 immune responses and their signature cytokines, IL-4, IL-5, and IL-13 in particular, are commonly observed during helminth parasitic infections. However, these same responses are also seen in a variety of allergic disorders.[1] Historically, type 2–associated responses were thought to be elicited primarily by multicellular organisms (eg, helminths) that were unable to be internalized by host cells and whose effector functions were believed to drive the development of humoral responses.[2] Indeed, it has been shown that IL-4 is crucial for human B-cell maturation and class switching to the IgE and IgG4 isotypes.[3-5] However, several studies have suggested that type 2–polarized T_H cells are more broadly defined and that the cells they target go well beyond B cells and include mast cells, basophils, and eosinophils.[2]

Studies of helminth infections and/or allergic diseases have helped to shape this redefinition of type 2–associated cell polarization; indeed, it is well known that T_H2 cell– and group 2 innate lymphoid cell (ILC)–associated cytokines are crucial for the recruitment and activation of eosinophils.[6,7] Of note, type 2–associated eosinophilic disorders (eg, lymphocytic variant hypereosinophilic syndrome, asthma, atopic dermatitis, drug hypersensitivity, helminth infection)[8] are defined by a marked recruitment of eosinophils to the tissue along with an extensive extracellular deposition of eosinophil-derived granule proteins. This eosinophil-rich inflammation has been shown to drive pathology in the affected organ.[9,10] Thus, because IL-5 has been designated as the key cytokine to induce eosinophilic inflammation, anti–IL-5 (mepolizumab) and IL5Rα-targeting (benralizumab) mAbs have been used as a novel therapeutic approach to target many of these eosinophil-dominated disorders.[11] Nevertheless, recent studies have proposed that other mediators, including IL-13 (independently or associated with IL-5), can also play a major role in the development of asthma and other eosinophilic disorders.[12,13] As a consequence, treatment approaches using a human mAb against IL-4Rα (dupilumab), which is a shared receptor for IL-4 and IL-13, have been tested in clinical trials in patients with asthma, chronic rhinosinusitis with nasal polyps, eosinophilic esophagitis, and/or atopic dermatitis.[14]

From [a]Laboratory of Parasitic Diseases, NIAID, National Institutes of Health, Bethesda, MD, [b]Laboratory of Immune System Biology, NIAID, National Institutes of Health, Bethesda, MD, [c]Laboratory of Molecular Immunology, NIAID, National Institutes of Health, Bethesda, MD, and [d]National Institute of Allergy and Infectious Diseases (NIAID) Collaborative Bioinformatics Resource, NIAID, National Institutes of Health, Bethesda, MD.

Received for publication December 15, 2022; revised April 19, 2023; accepted for publication April 30, 2023.

Available online June 26, 2023.

Corresponding author: Pedro Gazzinelli-Guimaraes, PhD, Laboratory of Parasitic Diseases, National Institute of Allergy and Infectious Diseases, 4 Center Dr, Building 4, Room 211 National Institutes of Health, Bethesda, MD 20892. E-mail: pedro.gazzinelliguimaraes@nih.gov.

The CrossMark symbol notifies online readers when updates have been made to the article such as errata or minor corrections

2772-8293

https://doi.org/10.1016/j.jacig.2023.100131

Abbreviations used
FITC: Fluorescein isothiocyanate
HDM: House dust mite
ILC: Innate lymphoid cell
KO: Knockout
OVA: Ovalbumin
WT: Wild-type

However, the upstream immunologic events that determine how IL-13–driven type 2 inflammation drives lung pathology still needs to be elucidated further.

Here, we demonstrate that house dust mite (HDM)-mediated allergic pulmonary inflammation is driven by a polyfunctional T_H2 effector cell immune response that leads to IL-13–driven inflammation. In addition, we find that eosinophil trafficking to HDM-sensitized lungs relies on production of IL-13–driven CCL-11 and CCL-24 by both fibroblasts and myeloid cells that orchestrate the pulmonary inflammation. In so doing, we have provided new insights into the dynamics (and controls) of eosinophil migration to the lung with allergy and shown how an eosinophilic-dominated type 2 inflammatory response in the pulmonary tree has important implications for bystander effects, including driving resistance to lung transiting helminth parasites.

METHODS

Mice

Wild-type (WT) C57/BL-6 mice and IL-5 knockout (KO) mice on a C57/BL6 genetic background (C57BL/6-Il5$^{tm1Kopf/J}$, male, aged 8 weeks, were purchased from The Jackson Laboratory (Bar Harbor, Me). TCR-α–deficient mice on a C57/BL-6 genetic background, WT BALB/c mice, IL-13Rα1 KO mice on a BALB/c genetic background, and IL-13Rα2 KO mice on a BALB/c genetic background (all male and aged 8 weeks), were purchased from Taconic Farms (Germantown, NY). ΔdblGATA mice (male and aged 8 weeks) on a BALB/c genetic background were provided by Helene Rosenberg of the Laboratory of Allergic Diseases, National Institute of Allergy and Infectious Diseases, National Institutes of Health, and bred in-house at the National Institutes of Health Animal Facility.

HDM-induced allergic inflammation

The mice were anesthetized with isoflurane and sensitized intranasally with 200 μg of *Dermatophagoides pteronyssinus* HDM extract (Greer Laboratories, Lenoir, NC) in 30 μL of PBS on day 0 and day 7. On days 14, 16, and 18, the mice were given 50 μg of HDM extract in a volume of 30 μL intranasally. For the analysis of immunopathology driven by inflammation due to HDM allergy, mice were humanely killed on day 20. For the interaction studies between HDM sensitization with *Ascaris* infection, mice were infected with *Ascaris* on day 18, immediately after the last sensitization with HDM by oral gavage. Tissues were examined immunologically on day 26 (8 days after infection, which corresponds with the peak of *Ascaris* larval migration in the lungs).

Experimental infection and parasitologic analysis

Mice were infected with *Ascaris suum* by intragastric inoculation of 2500 fully embryonated eggs, as previously described by Boes et al[15] and Gazzinelli-Guimaraes et al.[16] Parasite burden was evaluated as previously described.[16]

Morphometric analysis on the *Ascaris* larval stages

The development of *Ascaris* larval stages was evaluated by morphometric measurement of the length and width of the larvae recovered from the airways 8 days after infection, as previously described.[17] Morphometric analysis of the larvae was performed by using Imaris 9.0 software (Bitplane, Oxford Instruments, Abingdon, United Kingdom).

Naive $CD4^+$ T-cell purification and adoptive transfer

Naive $CD4^+$ T cells were isolated from a single-cell suspension from the spleens of 2 donor mice (C57/BL6 WT mice and IL-$5^{-/-}$ mice) by using the negative selection of the naive $CD4^+$ T-Cell Isolation Kit according to the manufacturer's protocol (Miltenyi Biotec, Gaithersburg, Md). Enriched naive $CD4^+$ T cells were tested to greater than 95% purity after isolation. After purification, 1×10^6 naive $CD4^+$ T cells from each donor were injected intraperitonially into their respective TCR-alpha KO recipient mice. A control group of recipient mice received PBS. After a 12-day waiting period to allow the newly transferred naive $CD4^+$ T cells (capable of producing IL-5 or not) to expand in the respective recipient mice, the allergic sensitization protocol was implemented.

Flow cytometry immunophenotyping

Lung tissue digestion was performed as previously described.[17,18] Leukocyte suspensions were then stained by using 2 panels of antibodies for flow cytometry: a $CD4^+$ T-cell polarization panel and a myeloid panel. For the $CD4^+$ T-cell panel, cells were incubated for 3 hours at 37°C in 5% CO_2 in the absence of (media) or after stimulation with 0.5/0.05 nM phorbol myristate acetate/ionomycin (Sigma-Aldrich, Burlington, Mass) and 10 μg/mL of brefeldin A. Briefly, staining using the T-cell polarization panel required 3 steps. The cells were stained with a LIVE/DEAD marker (Fixable Blue, UV450, Thermo Fisher Scientific). Second, after washing with FACS buffer (PBS, 2% FBS), antibodies against the extracellular markers CD45, TCR-β, and Thy1.2 were used. After washing, the cells were fixed with 4% paraformaldehyde and permeabilized (Perm buffer, eBiosciences) and finally stained with the following antibodies: CD4, CD154, IL-5, IL-13, IL-17A, and IFN-γ (see Table EI in the Online Repository at www.jaci-global.org). The myeloid panel was used *ex vivo* in a 2-step staining protocol: first, the cells were stained with a LIVE/DEAD marker (Fixable Blue, UV450, Thermo Fisher Scientific), and second, after washing with FACS buffer, CD11c, Ly6C, CD11b, MHC-II, Siglec F, Ly6G, and F4/80 were used (see Table E1). After washing, the cells were fixed with 4% paraformaldehyde. Data were acquired on an LSR Fortessa flow cytometer (BD Biosciences) and analyzed with FlowJo software (Tree Star).

Lung tissue chemokine, cytokine, and cytokine receptors

Lung tissue homogenates were prepared as previously described.[17] The lung tissue cytokines IL-4, IL-5, IL-6, IL-13, IL-17A, IL-33, IFN-γ, CCL-2, and M-CSF were measured by using a multiplex commercial kit according to the manufacturer's protocol (Millipore Sigma). The lung tissue chemokines CCL-11

(eotaxin 1) and CCL-24 (eotaxin 2) were measured by using a Duoset ELISA Kit (R&D Systems, Minneapolis, Minn). Lung IL-13Rα2 protein concentration was determined by ELISA as previously described.[19] High-protein-binding 96-well plates were coated with anti–IL-13Rα2 (1 μg/mL) (R&D Systems) in PBS overnight, and a biotinylated anti-mouse IL-13 (2 μg/mL; Centocor) was used for detection.

RNA purification from lungs with HDM allergy and nanostring analysis

In all, 9 lungs from HDM-allergen sensitized mice, and 9 lungs from naive mice were harvested and placed in a Precellys tube containing 500 μL of Trizol. The tissues were then homogenized by using a Precellys homogenizer. RNA capture and purification were performed by using a MagMAX-96 Total RNA Isolation Kit (Thermo Fisher, Waltham, Mass). RNA concentration (ng/μL) was determined by using a DeNovix DS-11 spectrophotometer. The purified RNA was divided into 3 pools from 3 mice each for each condition. After that, the preparation, hybridization, and detection of the RNA samples were carried out by following Nanostring manufacturer's instructions (Nanostring Technologies, Seattle, Wash). Subsequent analyses were performed by using thew nCounter Analysis System and TM4 MeV microarray software suite. The canonic signaling pathways in lungs with HDM allergy was analyzed by using Ingenuity Pathway Analysis (Qiagen, Hilden, Germany). The full list of genes analyzed by Nanostring, along with their respective expression levels in the lungs from naive mice and mice with HDM allergy, is available in Supplementary Data Set 1 (in the Online Repository at www.jaci-global.org).

Single-cell RNA sequencing and data processing

We generated a 10× Genomics Single-Cell Chromium mRNA library from $CD45^+$-sorted cells from mouse lungs of 3 HDM-sensitized mice and 3 naive mice. During this process we assigned a unique hashtag to each mouse before pooling samples into an HDM-positive pool and an HDM-negative pool. We sequenced these samples on 1 NovaSeq S2 and NovaSeq SP run at the Frederick National Laboratory for Cancer Research Sequencing Facility. Both samples have sequencing yields of more than 206 million reads per sample. The sequencing run was set up as a 28-cycles plus 91-cycle nonsymmetric run. When demultiplexing, we allowed 1 mismatch in the barcodes. The sequencing quality was good: more than 93.7% of bases in the barcode regions have Q30 or higher, at least 89.8% of bases in the RNA read have Q30 or higher, and more than 93.8% of bases in the unique molecular identifiers have Q30 or higher. We used Cell Ranger version 6.0.2[20] to analyze the data, following default parameters and mapping to the *Mus musculus* Genome Reference Consortium Mouse Build 38 (mm10, accession no. GCA_000001635.2; https://www.ncbi.nlm.nih.gov/assembly/GCF_000001635.20/).

After using Cellranger version 6.0.2 for alignment to mm10, followed by the quantification of RNA counts per cell, we used Seurat version 4.1.1[21] to filter the data and perform downstream analyses. We first visualized each data set to ensure that there was not a bimodal distribution with an excess of cells with multiple hashtags. We also used this software to determine the best cutoffs for cells that lacked unique features or had too many features and thus might may contain information on multiple cells. We retained cells with more than 200 unique features but fewer than 3000, and with less than 5% of reads mapping to mitochondrial genes. This resulted in 7077 cells with a mean of 1903 unique genes per cell in the HDM-negative sample and 3124 cells with a mean of 1355 unique genes per cell for the HDM-positive sample.

After filtering, we integrated samples based on the variable features of each cell and then clustered cells, following the default clustering parameters but with a resolution of 0.3. We then identified cell types in the integrated data set by using the ImmGen database in SingleR v1.8.1[22] and used Seurat v4.1.1 to generate dimension plots showing clusters and cell types of these data, as well as to generate features plots for differential markers expression level. For sets of differential markers in specific clusters or subclusters, we also generated heatmaps and volcano plots by using ggplot2 v3.3.6. Single-cell RNA sequencing data sets for both naive and HDM-sensitized $CD45^+$-sorted lung cells are available at the Gene Expression Omnibus GEO (accession nos. GSM6617107 and GSM6617109).

To see the *Ccl11* expression from nonhematopoietic cells, publicly available single-cell RNA sequencing data sets (reference, National Center for Biotechnology Information accession no. PRJNA838071) were downloaded and only the data from HDM-negative and HDM-positive WT mice were selected. As described earlier in this article, for downstream analysis such as filtering (nFeature_RNA > 700; nCount_RNA < 20000; and percent.mt < 10), data integration, normalization, scaling, and clustering (resolution, 0.2), Seurat, version 4.1.1, was used again. For cluster identification, the expression pattern of the signature genes suggested in the article was examined. To overcome the dropout effect in single-cell data, we used the MAGIC package (2.0.3) with the default setting (k-nearest neighbor = 5; decay = 1) for *Ccl11* expression to provide better visualization owing to imputation of missing values.

In vitro settings for IL-13–induced CCL-11 and CCL-24

Cells from the mouse bronchial cell line MM14.Lu (*CRL-6382)* (American Type Culture Collection, Manassas, Va) were cultured at 1×10^5cells per well and stimulated in the absence (with PBS alone) or presence of 100 ng/mL of recombinant murine IL-4 (Prepotech, Cranbury, NJ), 100 ng/mL of recombinant murine IL-5 (Prepotech), and 100ng/mL of recombinant murine IL-13 (Prepotech) for 48 hours at 37°C in 5% CO_2. After incubation, CCL-11 and CCL-24 levels were measured in the culture supernatant by using the Duoset ELISA Kit (R&D Systems). To characterize the MM14.Lu cell lines as fibroblasts, an immunophenotypic analysis by flow cytometry was performed using allophycocyanin anti-mouse EpCAM, efluor450 anti-mouse CD31, alexa fluor 700 anti-mouse CD45, biotinylated anti-mouse CD140a antibodies, and BV605 streptavidin (see Fig E2, *A* in the Online Repository at www.jaci-global.org).

In vivo eosinophil trafficking assay

To investigate the capacity of IL-13 to directly induce eotaxins levels, as well as to trigger eosinophilia in mouse lungs, 10 μg of recombinant murine IL-13 (Prepotech) was administered intranasally daily for 7 days. On day 4, after 3 doses of rIL-13, CCL-11

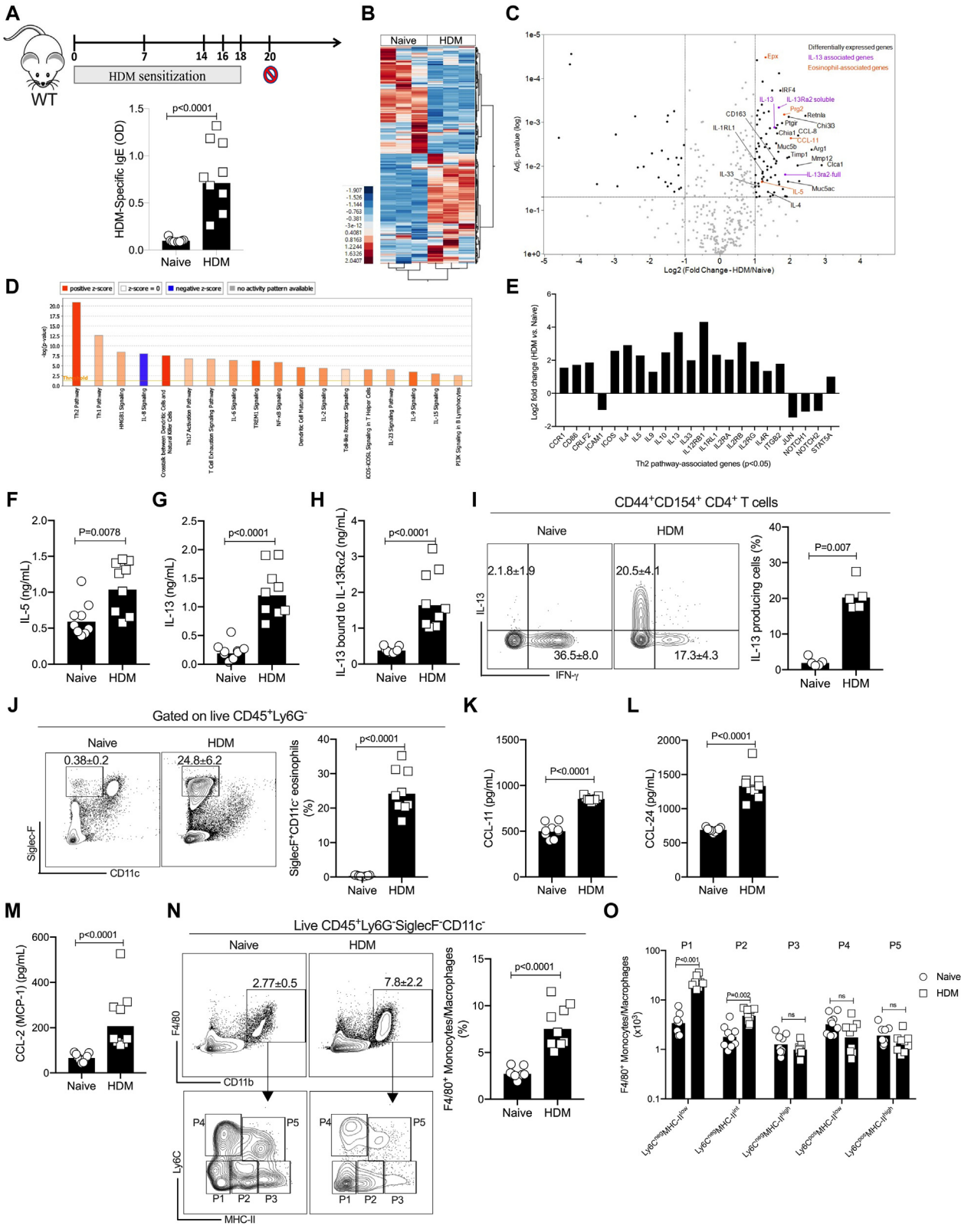

FIG 1. Sensitization with HDM allergen activates IL-13 signaling pathways and eotaxin levels and induces eosinophils' influx into the lung. Experimental design scheme for a murine asthma model driven by HDM allergen intranasal senstitization, and HDM allergen–specific IgE levels in naive mice (n = 9) versus in HDM-allergic mice (n = 9) on day 20, which was 2 days after the fifth and last sensitization (**A**). Heatmap with the differentially expressed genes, normalized by their *z* score, in lungs from naive mice and allergic animals, highlighting their distinct transcriptional signature (**B**). Significant ($P < .05$) upregulated and downregulated genes, with the $\log_2$ fold change threshold of greater than –1 or greater than 1, in the lungs of HDM-

and CCL-24 levels were measured in the lung homogenate by using the Duoset ELISA Kit (R&D Systems). On day 8, lungs were digested for flow cytometric analysis to evaluate the frequency of Siglec F–positive eosinophils by using a myeloid panel (see Table E1). In parallel, to test the capacity of IL-13 to traffic eosinophils from the circulation to the lung tissue, peripheral eosinophilia was induced by intraperitoneal injections of recombinant mouse IL-5 (Prepotech), 3 μg/mouse per day for 6 days. Intraperitoneal injections of PBS were used as a control. Blood was collected from the tail vein on days –6, –3, and 0 to track eosinophil counts using a hematology analyzer Element HT5 (Heska, Loveland, Colo). On day 0, mice received 3 consecutive intranasal injections of rIL-13 or PBS. On day 3, lungs were digested for flow cytometric analysis to evaluate the frequency of Siglec F–positive eosinophils. Of note, 5 to 10 minutes before the lung harvest, the anesthetized mice received intravascular injection of 1.25 μg of anti-mouse CD45–fluorescein isothiocyanate (FITC) in 200 μL of PBS, to discriminate between the cells in the pulmonary vascular circulation and those in the lung parenchyma.

Antibody response

IgG1, IgG2a, and IgE responses to HDM extract were evaluated as previously described.[17,18] Immulon ELISA 4HBX plates were coated with 5 μg of HDM extract (Greer Laboratories) per well.

Statistical analyses

Unless stated otherwise, the experimental results are represented as means plus or minus SEs or geometric means. For nonparametric data, the Kruskal-Wallis test followed by the Dunn multiple comparisons test was used for the analysis of tissue cytokine and chemokine profiles, the frequencies of myeloid and T cells, and the comparison of parasite burden and larval development between different mouse strains. Correlation analysis was performed by using the Spearman rank test. For both statistical tests, P values less than .05 were deemed statistically significant. P values are indicated in each graph, with *ns* denoting values that were not significant.

Study approval

All animal experiments were approved by the National Institutes of Health Animal Care and Use Committee (Animal Study Protocol LPD-6).

RESULTS

Environmental aeroallergen sensitization activates IL-13 signaling pathways, eotaxin levels, and influx of eosinophils to the lung

To dissect the pathways altered in HDM-driven pulmonary inflammation, we performed comprehensive transcriptional and immunologic profiling in the lungs of HDM-sensitized and naive mice (Fig 1). After confirming that the intranasal sensitization with HDM was successful by demonstrating increased HDM-specific IgE responses in the HDM-sensitized mice over naive animals, (0.795 ± 0.362 OD vs 0.098 ± 0.021 OD [$P < .0001$] [Fig 1, *A*]), we assessed the mRNA profile of the lungs driven by HDM allergens (Fig 1, *B*). Among the 171 differentially expressed genes (Fig 1, *C*), we observed overexpression of *Rtnla, Arg1, Muc5b, Irf4, Ptgir, Cd163,* and *Il1rl1* transcripts, among others (Fig 1, *E*). Remarkably, IL-13–associated genes, including *Il13* and *Il13ra2* (because IL-13 levels upregulate the expression of IL-13Rα2), as well as genes associated with eosinophil activation—namely, *Epx* (eosinophil peroxidase), *Prg2* (major basic protein), *Ccl-11* (eotaxin-1), and *Il-5*—were also markedly upregulated in the HDM-driven allergic pulmonary inflammation. Ingenuity Pathway Analysis (IPA) revealed a significant upregulation in the genes associated with T_H2 cell activation (Fig 1, *D*), including *Il4, Il4rα, Il5, Il9, Il13, Il33,* and *Itgb2* (Fig 1, *E*). At the protein level, HDM-sensitized lung homogenates showed significant increases in abundance of IL-5 (Fig 1, *F*), IL-13 (Fig 1, *G*), and IL-13-bound to IL-13Rα2 (Fig 1, *H*) versus in homogenates of lungs from naive mice. The immunophenotypic analysis of lung tissue cells revealed a marked expansion of effector memory $CD4^+$ T cells producing IL-13 following HDM sensitization (Fig 1, *I*). Moreover, we found that the cellular composition of the lung tissue was marked by a profound influx of eosinophils (Fig 1, *J*) and was associated with a marked increase in CCL-11 (855.3 ± 8.85 pg/mL vs 507.6 ± 26.45 pg/mL [$P < .0001$] [Fig 1, *K*]) and CCL-24 (eotaxin-2) (1345.0 ± 209.7 pg/mL vs 691.2 ± 30.6 pg/mL [$P < .0001$] [Fig 1, *L*]). Finally, our analysis of other chemokines also showed a marked increase in CCL-2 levels (monocyte chemoattractant protein-1 (MCP-1) (Fig 1, *M*), indicating a potential increase in monocytic populations driven by HDM sensitization. Indeed, flow cytometric analysis showed a significant increase in the frequency of $F4/80^+$ monocytes/macrophages in the allergen-sensitized lungs (Fig 1, *N*), characterized by an increase in the absolute numbers of nonclassical $Ly6C^-MHCII^-$ ($P < .001$) and $Ly6C^-MHCII^{int}$ ($P = .002$) monocytes but similar numbers of classical $Ly6C^+$ monocytes when compared with the levels in the lungs from naive mice (Fig 1, *O*).

sensitized mice over those in lungs from naive mice obtained from a nanostring analysis of 507 genes associated with inflammation (**C**). T_H2 cell pathway–associated genes that overlap with the marked differentially expressed genes in the lungs from HDM-sensitized mice over those in the lungs obtained from naive mice (**D** and **E**). Pulmonary tissue levels of IL-5 (**F**), IL-13 (**G**), IL-13 bound to IL-13R*a2* (**H**), CCL-11 (**K**), CCL-24 (**L**), and CCL-2 (**M**) in the lung homogenates obtained from naive BALB/c mice and from BALB/c mice with HDM-allergic inflammation (n = 9 mice per group). Representative flow cytometry dot plot of lung cells (n = 5 in each group) stimulated with phorbol myristate acetate (PMA)/ionomycin for 3 hours, gated on $CD44^+CD154^+TCR\text{-}\beta^+CD4^+$ T cells, showing the frequencies of IL-13 and IFN-γ, followed by the frequency of IL-13–producing effector memory $CD4^+$ T cells (**I**). Representative flow cytometry dot plots of the lungs, gated on $CD45^+Ly6G^-$, showing the frequencies of Siglec F–positive $CD11c^-$ eosinophils (**J**) and a representative flow cytometry dot plot of the lungs showing the frequencies of $CD11b^+F4/80^+$ macrophages expressing Ly6C and/or MHC-II (**N**). Absolute number of different clusters of macrophages in lungs from naive mice and lungs from HDM-sensitized mice (**O**). Each symbol represents a single mouse, and horizontal bars are geometric means. P values are indicated on each graph. Two independent experiments were performed. Differences between the naive and HDM groups were considered statistically significant at P values less than .05 obtained by the unpaired Mann-Whitney test. **D,** generated by QIAGEN Ingenuity Pathway Analysis software.

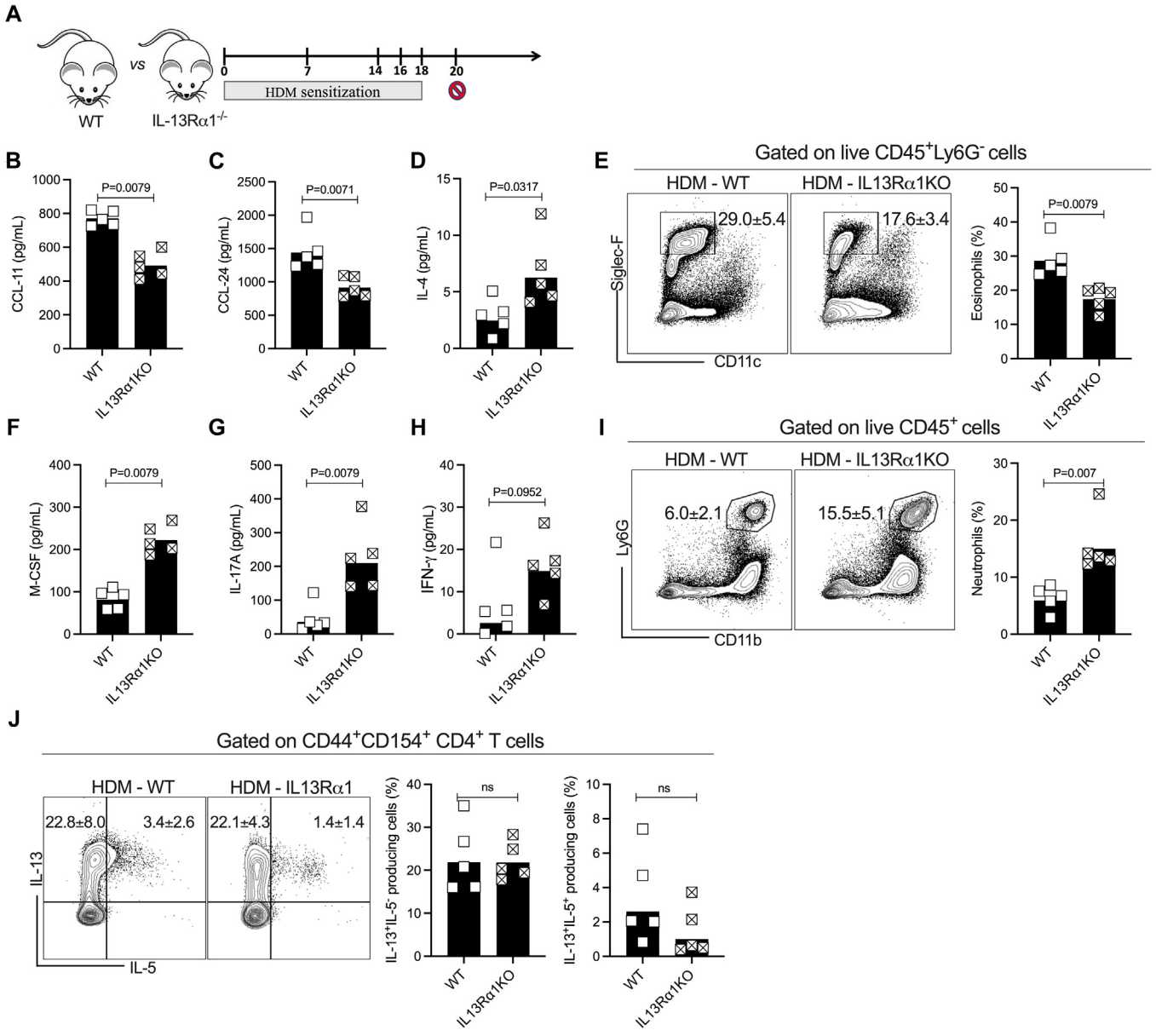

FIG 2. Absence of IL-13 signaling in IL-13Rα1 KO mice impairs eosinophil-dominated type 2 inflammation driven by HDM sensitization. Experimental design scheme for HDM-allergen sensitization in WT (n = 5) and IL-13Rα1 KO (n = 5) mice (**A**). Pulmonary tissue levels of CCL-11 (**B**), CCL-24 (**C**), IL-4 (**D**), macrophage colony-stimulating factor (M-CSF) (**F**), IL-17A (**G**), and IFN-γ (**H**) in the lung's homogenates of HDM-sensitized WT and IL-13Rα1 KO mice. Representative flow cytometry dot plots of lungs cells, gated on live $CD45^+Ly6G^-$, showing the frequencies of Siglec F–positive $CD11c^-$ eosinophils (**E**) and lung cells, gated on live $CD45^+$, showing the frequencies of $Ly6G^+CD11b^+$ neutrophils (**I**). Representative flow cytometry dot plot of lung cells from both HDM-sensitized WT and IL-13Ra1 KO lungs stimulated with phorbol myristate acetate (PMA)/ionomycin for 2.5 hours, showing the frequencies of $CD44^+CD154^+CD4^+$ T cells producing either IL-5 or IL-13 (**J**). Each symbol represents a single mouse, and horizontal bars are geometric means. *P* values are indicated on each graph. Two independent experiments were performed. Differences between the 2 groups were considered statistically significant at *P* values less than .05 obtained by the unpaired Mann-Whitney test.

Allergen-driven eosinophil-dominated type 2 allergic inflammation in the lungs relies on IL-13 signaling

Having observed that inflammation in the lungs driven by HDM sensitization was characterized by an increase in IL-13–producing $CD4^+$ T-cell and elevated IL-13 levels in the lung tissue, we next explored the role of IL-13 signaling in the lung eosinophils of mice with allergy. By comparing the allergic pulmonary inflammation in HDM-sensitized WT mice with that in IL-13Rα1$^{-/-}$ mice (Fig 2, *A*), we demonstrated that in the absence of IL-13 signaling, sensitization due to HDM allergy showed a marked increase in the levels of both CCL-11 (771.9 ± 19.3 pg/mL vs 496.6 ± 34.5 pg/mL [P = .0079] [Fig 2, *B*]) and CCL-24 (1461.0 ± 133.4 pg/mL vs 923.7 ± 68.1 pg/mL [P =

.0071] [Fig 2, *C*]) from WT mice versus IL-13Rα1$^{-/-}$ mice, respectively. Interestingly, the IL-4 levels in the HDM-sensitized IL-13Rα1$^{-/-}$ mice were significantly increased when compared with those in the lungs from the HDM group (Fig 2, *D*). The impaired production of CCL-11 and CCL-24 in the lung tissue of IL-13Rα1$^{-/-}$ mice with allergic inflammation was associated with a marked reduction in the frequency of eosinophils in the lung tissue ($P = .0079$) (Fig 2, *E*). Furthermore, HDM-sensitized IL-13Rα1$^{-/-}$ lungs showed a clear alteration of the T_H2 cell–T_H1 cell–T_H17 cell balance, with a shift away from a type 2 phenotype toward a mixed type 1/type 17 response with elevated levels of M-CSF (224.3 ± 33.53 pg/mL vs 83.8 ± 23.2 pg/mL [$P = .0079$] [Fig 2, *F*]), IL-17A (225.0 ± 96.3 pg/mL vs 46.6 ± 43.0 pg/mL [$P = .0079$] [Fig 2, *G*]), and IFN-γ (16.2 ± 6.9 pg/mL vs 6.8 ± 8.6 pg/mL [$P = .0950$] [Fig 2, *H*]) versus in HDM-sensitized WT mice. Moreover, this mixed type 1 and type 17 responses observed in the HDM-sensitized IL-13Rα1$^{-/-}$ mice was also characterized by a marked increase in number of neutrophils in the lungs when compared with the number in the lungs of WT mice with allergy ($P = .007$ [Fig 2, *I*]). Of note, the lack of IL-13 signaling did not alter the frequency of HDM-driven IL-5$^+$ and/or IL-13$^+$–producing T_H2 effector cells (Fig 2, *J*).

Single-cell resolution of HDM-driven pulmonary allergic inflammation reveals the major sources of IL-13, CCL-11, and CCL-24

To understand (at single-cell resolution) how allergen sensitization reshapes the transcriptional profile of the lung populations, we performed single-cell RNA sequencing data from sorted CD45$^+$ lung cells from HDM-sensitized mice and lungs from naive mice. We clustered lung cells on the basis of their expression profile by using Seurat and annotated fine cell types on the ImmGen mouse database[23] using SingleR. Overall, we identified a total of 13 clusters in the lung cells, corresponding to the major clusters of hematopoietic cells (Fig 3, *A*). We then evaluated the expression levels of *Il13, Il4, Il5, Il13rα1, Il4rα, Ccl11*, and *Ccl24* in the different clusters based on the allergic status of the mice (see Fig E1 in the Online Repository at www.jaci-global.org). In the lung cells from naive mice, we observed that *IL13* transcripts were restricted to ILCs (cluster 10) and basophils/mast cells (cluster 12). We also found CD4$^+$ T cells expressed low levels of *IL4* in lung cells from naive mice, but *Il4* appeared to be expressed at high levels only on basophils/mast cells. *IL5* was predominantly expressed only on the ILC cluster, with no expression on CD4$^+$ T cells or basophils/mast cells in naive CD45$^+$ lung cells. Surprisingly, we found that *Il13rα1* expression levels were restricted to neutrophils (cluster 5) and the monocyte/macrophage clusters (cluster 6), whereas at baseline, *Il4rα* was expressed in all major clusters of CD45$^+$ lung cells. At baseline, *CCL24* was expressed on natural killer cells (cluster 3) and ILCs at a high level but also on neutrophils and B cells (cluster 0) at low levels. Remarkably, the HDM sensitization altered considerably the expression dynamics of these markers among the hematopoietic lung cells. Not only did HDM sensitization induce a marked increase in the expression level of *Il13*, *Il4*, and *Il5* among the CD4$^+$ T cells (cluster 1), but (as observed in Fig 2, *I* for IL-5 and IL-13) it seems that many of these effector CD4$^+$ T cells became polyfunctional (IL-4$^+$/IL-5$^+$/IL13$^+$). Moreover, *Il-13rα1* expression levels continued to be restricted to neutrophils and monocytes/macrophages, and Il4rα expression levels changed only slightly after HDM sensitization. A major change driven by the allergen sensitization, however, involved *CCL24* expression, which was restricted to CD4$^+$ T cells, ILCs, and myeloid cells (monocyte/macrophage cluster) in HDM-treated lungs (see Fig E1).

Because the monocyte/macrophage cluster expresses both *Il13rα1* and *Ccl24* in the HDM-sensitized lungs (CD4$^+$ T cells do not express *Il13rα1*), we sought to elucidate the eotaxin-2–producing myeloid cells in the lungs from mice with allergy. By subclustering *Cd11b*-expressing cells (from cluster 6) using SingleR, we identified 6 subclusters (P0-P5) within the monocyte/macrophage cluster (Fig 3, *A*). On the basis of the top 20 overexpressed genes for each subcluster (Fig 3, *B*) along with the expression level of *Ccr2*, *Ly6c*, *Fcgr1 (CD64)*, *Cx3cr1*, *Spn (CD43),* and *Fcgr4 (CD16-2)* (Fig 3, *C*) it was possible to annotate the 6 subclusters as follows: P0 and P1, CCR2$^-$*Cx3cr1*$^+$*Spn*$^+$*Fgr4*$^+$*Nr4a1*$^+$*Ly6C*$^-$ nonclassical patrolling monocytes; P2, *Ccr22*$^+$*Fcgr1*$^+$*F13a1*$^+$*Vcan*$^+$*Ly6C*$^+$ classical monocytes; P3 and P4, dendritic cells; and P5, interstitial macrophages. Within the 6 subclusters (Fig 3, *D*), we found that only classical *Ly6c*$^+$ monocytes could express *Ccl24* (Fig 3, *E* and *F*).

Of note, *Ccl11* expression was not detected in any CD45$^+$ cell type in either the HDM-negative or HDM-positive lungs, suggesting that eotaxin-1 is expressed largely by nonhematopoietic compartment in lungs from mice with allergy. To investigate whether any other lung tissue compartments could express levels of *Ccl-11* driven by HDM sensitization, we reanalyzed publicly available single-cell RNA sequencing data regarding lungs from naive mice and lungs from HDM-sensitized mice containing epithelial, stromal, and mesenchymal cells[24] (Fig 3, *G*). The analysis revealed elevated expression levels of *Ccl11* restricted to lung fibroblasts (*Col1a1*, *Col1a2*, *Col3a1*, *Fbln1*, and *Pdgfra* [*CD140a*]) in the lungs from mice with HDM allergy. Eotaxin-1 expression levels were markedly increased in comparison with the levels in lung fibroblasts from naive mice (Fig 3, *H*). Notably, *Ccl24* expression was not detected in any nonhematopoietic cell type. To test the capacity of lung bronchial fibroblasts to produce CCL-11 in response to IL-13, we stimulated a mouse bronchial fibroblasts cell line (MMP14.Lu) (EpCAM$^-$CD31$^-$CD45$^-$CD140a$^+$ [see Fig E2, *A*]) in the absence or in the presence of rIL-4, rIL-5, or rIL-13. Interestingly, rIL-13 induced a remarkable amount of CCL-11 (402.6 ± 37.4 pg/mL vs 7.26 ± 7.3 pg/mL [$P = .0187$] [Fig E2, *B*]), when compared with the amounts in unstimulated cells (PBS) and cells stimulated with the other T_H2 cell–associated cytokines. None of the conditions induced any CCL-24 in this bronchial fibroblast cell line (Fig E2, *C*), suggesting that the fibroblasts are indeed a major source of CCL-11 in lungs from mice with HDM allergy (but not CCL-24) in response to IL-13 signaling.

IL-13–mediated eotaxin-dependent eosinophil influx to the lung tissue requires peripheral eosinophilia

So far, we have shown that IL-13 is one of the major components of HDM-driven pulmonary allergic inflammation and that eosinophils largely fail to migrate to lungs from mice with allergy in the absence of IL-13 signaling. On the basis of these results, we then hypothesized that IL-13 promotes eosinophil influx to the lung tissue by eotaxin-mediated trafficking. Because many other mediators besides IL-13 induced by HDM sensitization could

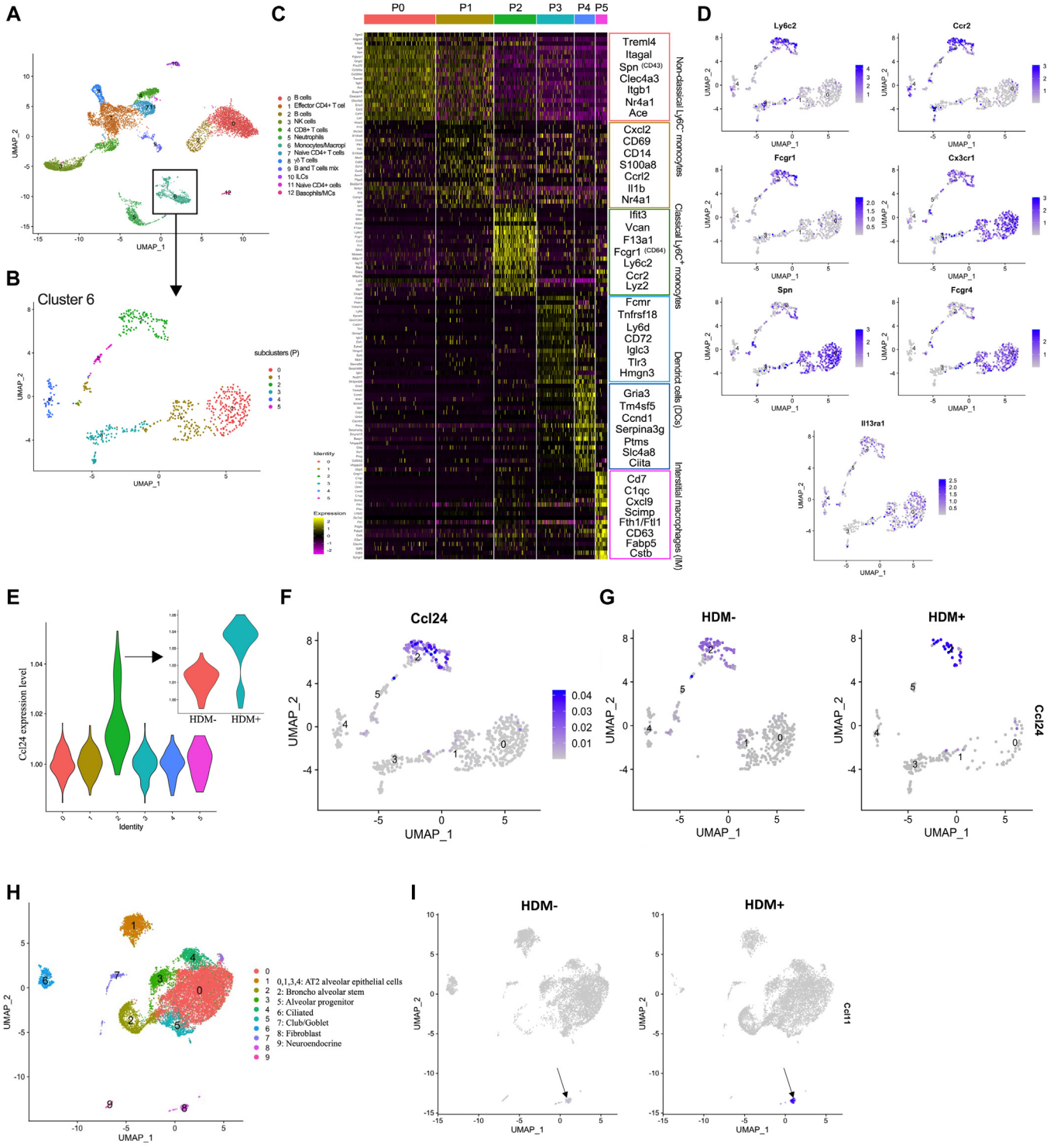

FIG 3. Single-cell RNA sequencing analysis of lungs from HDM-sensitized mice reveals the major sources of CCL-11 and CCL-24. From CD45^{+}-sorted cells of lungs from naive mice (n = 3) and lungs with allergic inflammation (n = 3), a total of 13 clusters of hematopoietic cells were identified on the basis of their expression profile using Seurat and annotated fine cell types on the ImmGen mouse database using SingleR (**A**). The monocyte/macrophage cluster (cluster 6) was subclustered in 6 populations (**B**), which were further characterized in the heatmap based on the top 20 upregulated genes of each subpopulation (**C**). Uniform Manifold Approximation and Projection plots with the levels of expression from signature genes for classical Ly6C^{+} monocytes, including *Ly6c2, Ccr2,* and *Fcgr1* (CD64), as well as nonclassical Ly6C^{-} monocytes, including *Cx3cr1*, *Fcgr4,* and *Spn* (CD43), were also analyzed for further cell type annotation (**D**). Expression level of CCL-24 was investigated among the myeloid subpopulations and compared between lung cells from naive mice and lung cells from mice with HDM allergy (**E-G**). Using publicly available single-cell RNA-sequencing data from CD31- and CD45-depleted cells of lungs from naive mice and lungs from mice with HDM allergy, a total of 9 clusters of epithelial, stromal, and mesenchymal cells were identified on the basis

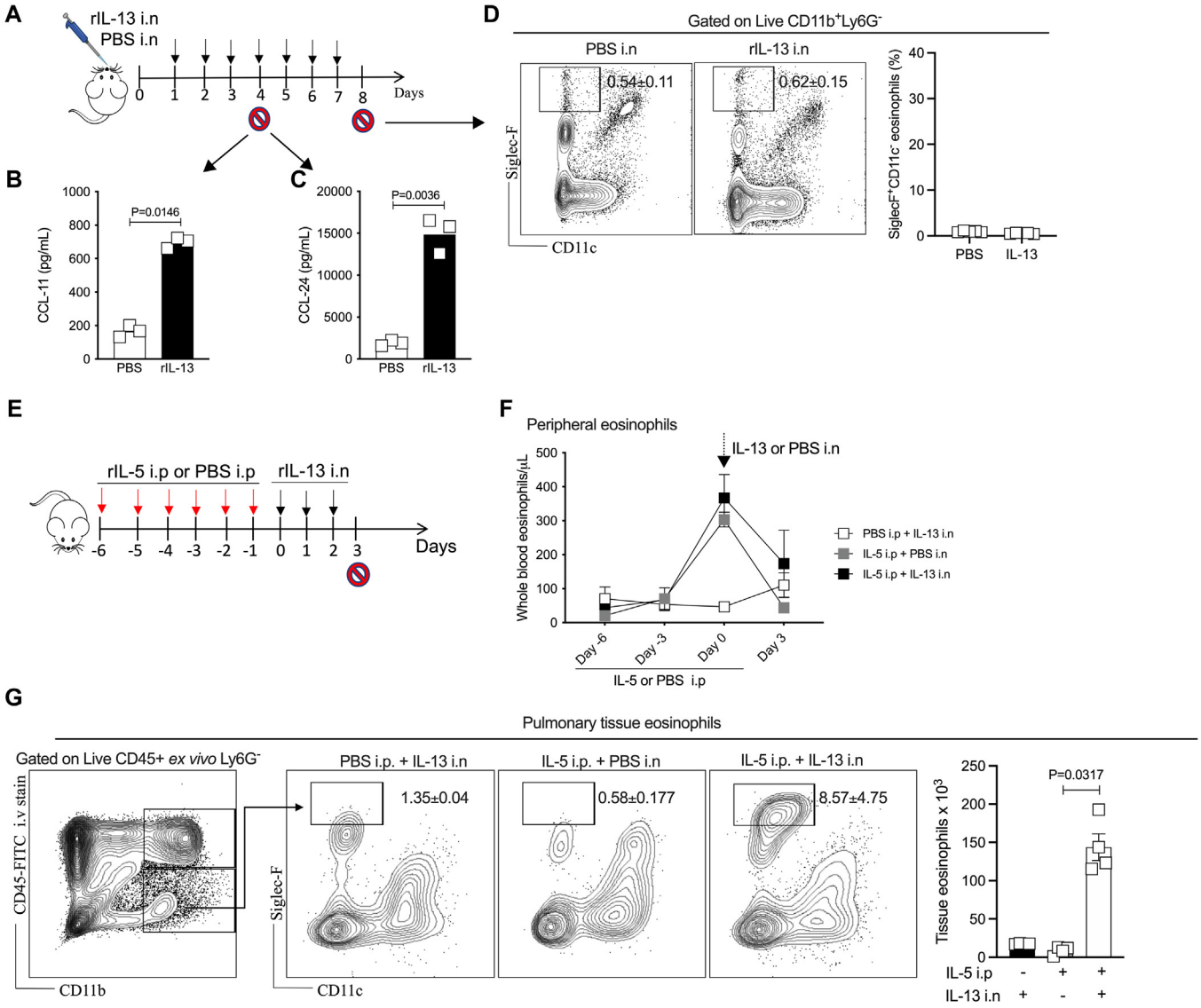

FIG 4. IL-13–mediated eotaxin-dependent eosinophil influx to the lung tissue requires peripheral eosinophilia. Either 10 μg of rIL-13 or PBS was administered intranasally to naive Balb/c mice for 7 days (n = 3) (**A**). On day 4 and after 3 injections of rIL-13, the levels of CCL-11 (**B**) and CCL-24 (**C**) in the lung homogenates were measured by ELISA. On day 8, the frequency of Siglec F–positive CD11c$^-$ eosinophils in the lungs was analyzed by flow cytometry (**D**). Experimental design for an *in vivo* assay to investigate eosinophil trafficking from the blood circulation to the lung tissue driven by recombinant T_H2 cytokines in Balb/c mice (n = 4). rIL-5 (3 μg/mouse per day for 6 days) was administered intraperitoneally, starting on day –6. Intraperitonal injections of PBS were used as a control (**E**). Peripheral blood was collected from the tail vein on days –6, –3, and 0 to track eosinophil counts. On day 0, mice received 3 consecutive intranasal injections of rIL-13 or PBS (**F**). On day 3, lungs were digested for flow cytometric analysis to evaluate the frequency of Siglec F–positive eosinophils. To discriminate between the eosinophils in the pulmonary vascular circulation (CD11b$^+$CD45i.v$^+$) and those in the lung parenchyma (CD11b$^+$CD45i.v$^-$), anesthetized mice received intravascular injection of 1.25 μg of anti-mouse CD45-FITC in 200 μL of PBS (**G**). Each symbol represents a single mouse, and the horizontal bars are the geometric means. *P* values are indicated on each graph. Three independent experiments were performed. Differences among the groups were considered statistically significant at *P* values less than .05 by the Kruskal-Wallis test followed by the Dunn multiple comparison test.

work redundantly, we next assessed whether intranasal administration of recombinant IL-13 in naive mice was, by itself, capable of inducing CCL-11 and CCL-24 in the lungs. Eotaxin-1 and eotaxin-2 levels were measured in the lung homogenates on day 4, following 3 consecutive doses of rIL-13 (10 μg/dose), and eosinophil frequency in the lung was assessed on day 8, after 7 doses of rIL-13 (Fig 4, *A*). The data show that rIL-13 per se induced a marked increase in CCL-11 (696.5 ± 18.2 pg/mL vs 166.7 ±

of their expression profile using Seurat and annotated fine cell types on the ImmGen mouse database using SingleR (**H**). Expression levels of CCL-11 and CCL-24 were investigated among the clusters and were compared between lung cells from naive mice and lung cells from HDM-allergic mice(**I**).

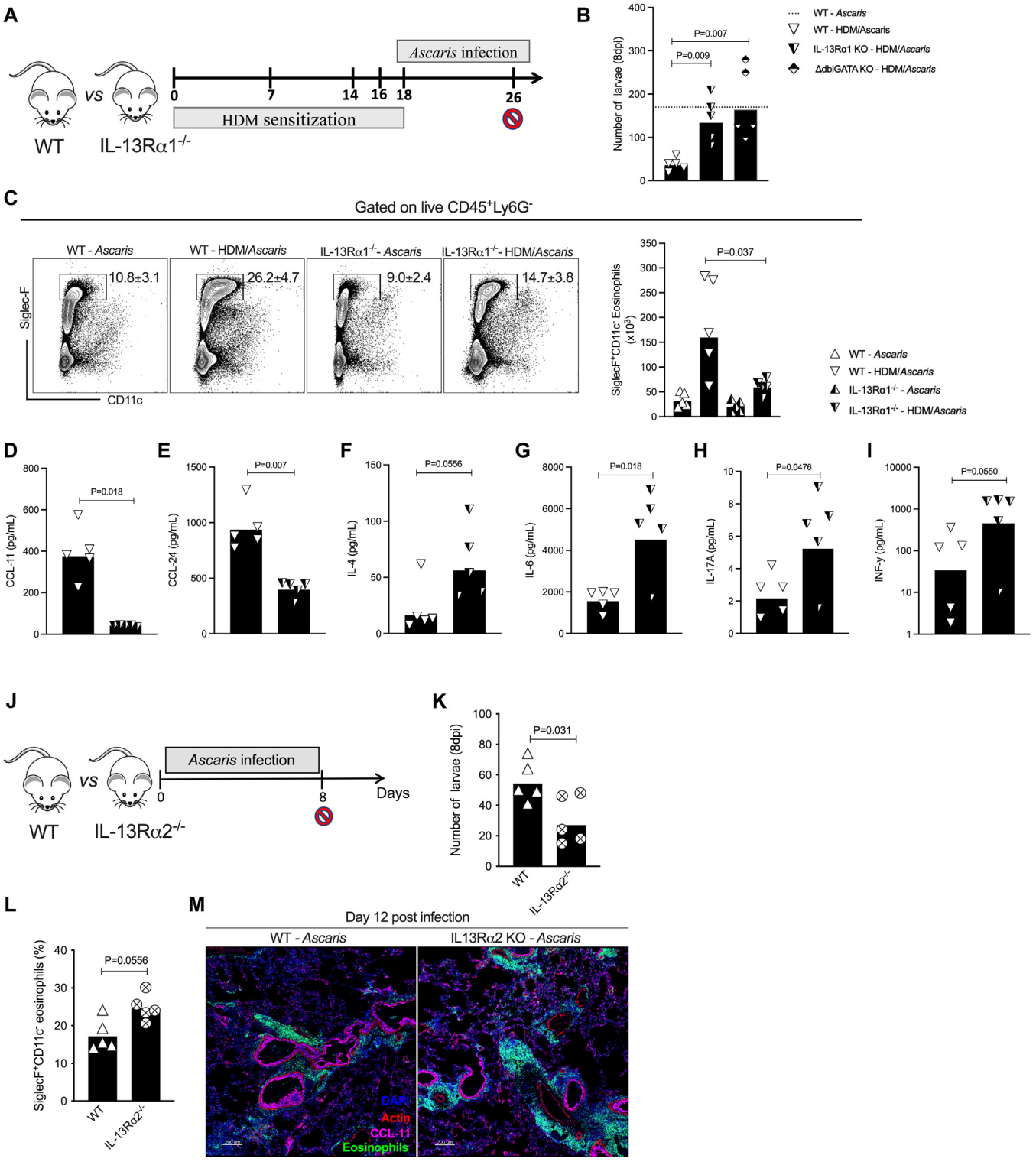

FIG 5. Bystander effect of allergen-induced IL-13–driven eosinophil-dominated type 2 inflammation protects the host from tissue-transiting helminth parasites. Experimental design scheme for HDM allergic sensitization followed by *Ascaris* infection in WT (n = 5) and IL-13Rα1 KO mice (n = 5) (**A**). Parasite burden in the lungs of allergy-free *Ascaris*-infected mice (n = 5) and HDM-sensitized mice followed by *Ascaris* infection in the presence (WT) (n = 5) or absence of IL-13 signaling (IL-13Rα1 KO) (n = 5) on day 8 of infection (**B**). Representative flow cytometry dot plots of lung cells showing the frequencies of Siglec F–positive $CD11c^{-}$ eosinophils in the different groups on day 8 and the absolute number of eosinophils by animal level and their respective groups (**C**). Pulmonary tissue levels of eotaxin-1 (CCL-11) (**D**), eotaxin-2 (CCL-24) (**E**), IL-4 (**F**), IL-6 (**G**), IL-17A (**H**), and IFN-γ (**I**) in the lung homogenates of HDM-sensitized/*Ascaris*-infected WT mice and HDM-sensitized/*Ascaris*-infected IL-13Rα1 KO mice. Experimental design scheme for *Ascaris*

19.7 pg/mL [$P = .0146$] [Fig 4, *B*]) and CCL-24 levels (14,967 ± 1,204 pg/mL vs 1915 ± 187.7 pg/mL [$P = .0036$] [Fig 4, *C*]) when compared with PBS intranasal administration.

Nevertheless, intranasal rIL-13 administration to naive mice failed to induce lung eosinophils on day 8 (Fig 4, *D*). However, if peripheral eosinophilia was induced before the intranasal administration of rIL-13 (Fig 4, *E* and *F*), it could be shown that IL-13–mediated eotaxins are capable of recruiting eosinophils to the lung tissue. Furthermore, using intravascular injection of anti-mouse CD45-FITC before lung harvest, we were able to confirm that the pulmonary eosinophils resided in the tissue and not in the vasculature, through gating on CD45-FITC–positive cells.

Bystander effects of HDM-driven IL-13/eotaxin production

We have previously shown that HDM-driven pulmonary allergic inflammation markedly limits helminth parasite numbers in lungs in a model of allergy/helminth coinfection.[17] To understand the role played by IL-13 in mediating host protection from pulmonary transiting parasites (eg, *Ascaris* spp), we infected HDM-sensitized WT and IL-13Rα1$^{-/-}$ mice with *Ascaris* parasites and evaluated the parasite burden and lung pathology during the peak of *Ascaris* larval migration (Fig 5, *A*). Inflammation in WT mice driven by HDM sensitization was associated with a dramatic reduction in the number of the lung-stage *Ascaris* larvae versus in *Ascaris*-infected WT mice without allergy (38 ± 6.63 larvae vs 170.2 ± 19.3 larvae [$P = .0003$]); in contrast HDM sensitization of IL-13Rα1–deficient mice were no longer able to control the number of pulmonary-trafficking *Ascaris* larvae (142.2 ± 53.7 larvae [$P = .009$] vs in WT mice with HDM allergy). In addition, the pulmonary allergic inflammation seen in the IL-13Rα1 KO mice was similar to that observed in eosinophil-deficient mice (ΔdblGATA); nor were there effects on limitation of *Ascaris* larval numbers or development (Fig 5, *B*).

Of note, there was a dramatic reduction ($P = .037$) in lung tissue eosinophil frequency and numbers in HDM-sensitized/*Ascaris*-infected IL-13Rα1–deficient mice versus in HDM-sensitized/*Ascaris*-infected WT animals (Fig 5, *C*). Further, this absence of IL-13 signaling in the epithelium of lung from allergic mice was associated with a marked suppression of CCL-11 levels (392.3 ± 124.2 pg/mL vs 41.1 ± 3.7 pg/mL [$P = .0018$] [Fig 5, *D*]) and CCL-24 levels (952.4 ± 202.4 pg/mL vs 403.1 ± 75.28 pg/mL [$P = .0070$] [Fig 5, *E*]). As observed for HDM sensitization in the absence of IL-13 signaling (Fig 2), the pulmonary inflammation driven by HDM sensitization/*Ascaris* infection in IL-13Rα1–deficient mice was characterized by an increase in IL-4 (Fig 5, *F*), as well as by a shift toward a mixed type 1 and type 17 response, with elevated levels of IL-6 (Fig 5, *G*), IL17-A (Fig 5, *H*), and IFN-γ (Fig 5, *I*) versus the levels in HDM-sensitized/*Ascaris*-infected WT mice. This alteration in the nature of HDM-driven inflammation in the absence of IL-13 signaling was also supported by the alterations in the antibody response against HDM (see Fig E3 in the Online Repository at www.jaci-global.org), as HDM sensitization in IL-13Rα1 KO mice showed increased HDM-specific IgG2 levels (see Fig E3, *B*) and diminished IgE levels (Fig E3, *C*) versus the levels in HDM-sensitized WT mice. No changes in IgG1 levels were observed.

Together, these data suggest that the IL-13/IL-13Rα1 axis in the HDM-sensitized lung tissue controls the number of eosinophils in an eotaxin-dependent manner. Conversely, lungs of *Ascaris*-infected IL-13Rα2 KO mice (Fig 5, *J*), which exhibit increased bioavailability of IL-13 owing to the absence of the decoy IL-13Rα2, showed a marked reduction in the number of *Ascaris* larvae (55.6 ± 13.2 larvae vs 30.2 ± 15.6 larvae [$P > .031$] [Fig 5, *K*]). This finding was associated with a significant increase in the frequency of eosinophils versus that in *Ascaris*-infected WT mice, as evidenced both by flow cytometry and by confocal evaluation of tissue sections (Fig 5, *L* and *M*). Interestingly, as opposed to what we observed in the case of HDM-driven pulmonary allergic inflammation, which indicated that CCL-11 production seems to be restricted to bronchial fibroblasts, the confocal imaging of the lungs from both *Ascaris*-infected WT and IL-13Rα2 KO mice during the peak of larval migration revealed that CCL-11 staining was also colocalized with the bronchial epithelial cells in the lungs, suggesting that early in the infection by pulmonary helminth parasites, the epithelial compartment can also be an important source of eotaxin-1.

IL-13–mediated eosinophil-dependent helminth larval killing relies on allergen-driven IL-5–producing T_H2 effector cells

Because we showed that HDM sensitization induces a polyfunctional IL-5$^+$IL-13$^+$CD4$^+$ T cells, and that the downstream IL-13–mediated eotaxin-dependent eosinophil influx to the lung tissue requires a preceded IL-5–induced peripheral eosinophilia, we sought to investigate the role played by tissue-resident IL-5$^+$ and/or IL-13$^+$ T_H2 cells in mediating the eosinophil-dependent helminth larval killing in allergic lungs.

We first adoptively transferred naive CD4$^+$ T cells from either WT or IL-5–deficient mice into TCRα-deficient recipient mice in the context of HDM sensitization and/or *Ascaris* infection (Fig 6, *A* and *B*). After 12 days (allowing for expansion of transferred CD4$^+$ T cells), we assessed the role of IL-5–producing CD4$^+$ T cells in mediating the HDM-driven eosinophil-dependent inflammation in limiting the tissue trafficking *Ascaris* larvae. Interestingly, the absence of naive IL-5–producing CD4$^+$ T cells before the sensitization due to HDM allergy significantly impaired not only the differentiation of IL-5$^+$IL-13$^-$ T_H2 cells

infection in WT and IL-13Rα2 KO mice (**J**). Parasite burden in the lungs of *Ascaris*-infected WT and IL-13Rα2 KO mice on day 8 of infection (**K**). Flow cytometry analysis in the lungs of *Ascaris*-infected WT and mice IL-13Rα2 KO mice on day 8 of infection, indicating the frequency of Siglec–positive CD11c$^-$ eosinophils (**L**). Representative confocal panel of a lung section from *Ascaris*-infected WT (*left*) and mice IL-13Rα2 KO mice (*right*) on day 12 after infection stained with 4′,6-diamino-2-phenylindole, AF546 anti–CCL-11, and FITC anti–Siglec F, highlighting the number of peribronchial and perivascular eosinophils in the lungs of IL-13Ra2 KO mice in green. Each symbol represents a single mouse, and horizontal bars are geometric means. *P* value is indicated in each graph. Three independent experiments were performed. The Kruskal-Wallis test followed by the Dunn multiple comparison test was used for comparisons in (**B**) and (**C**). For all other graphs, differences between the 2 groups were considered statistically significant at *P* values less than .05 obtained by the unpaired Mann-Whitney test.

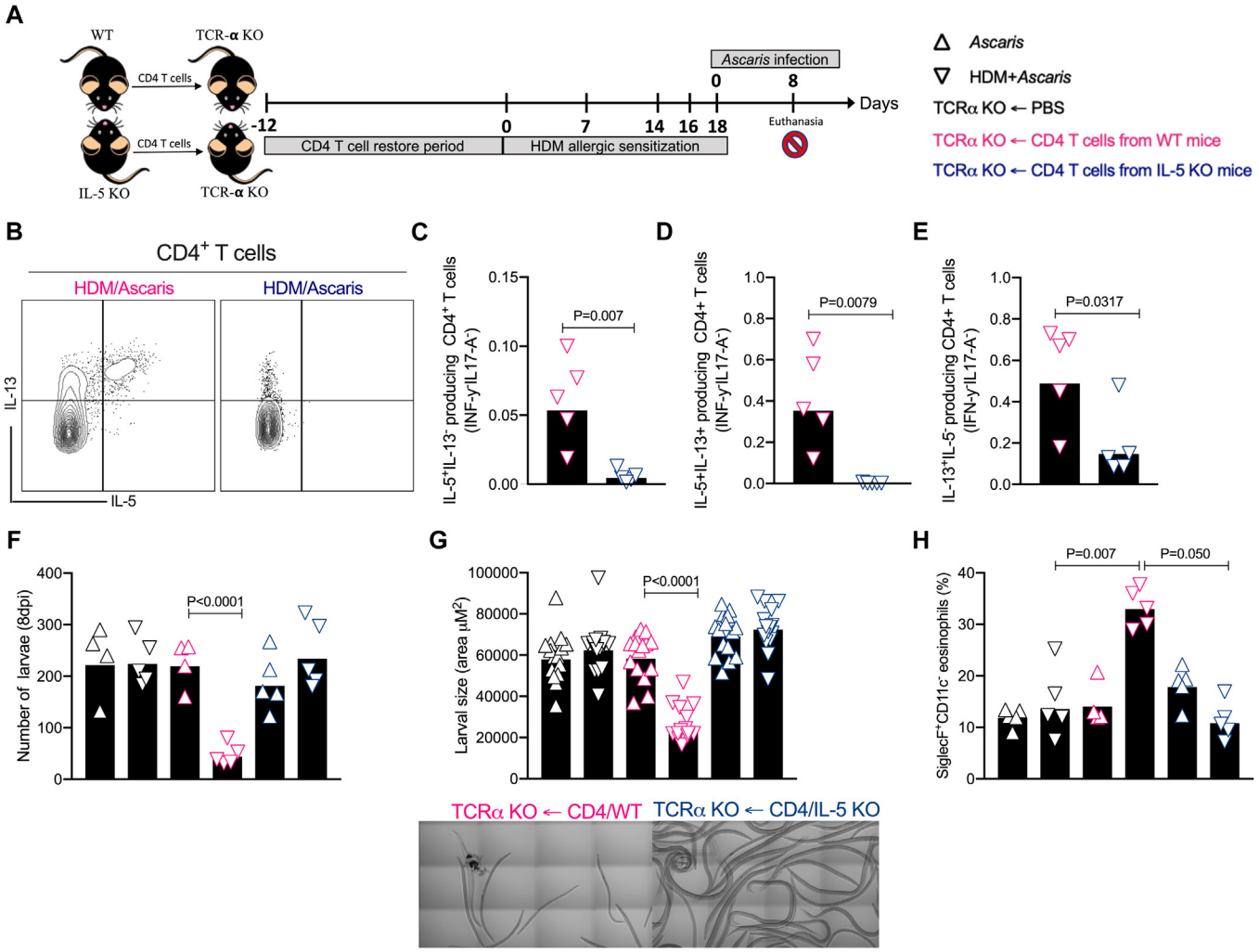

FIG 6. IL-5–producing CD4$^+$ T_H2 cells driven by pulmonary allergic inflammation promote an eosinophil-associated arrest on helminth larval development in the lungs. Spleen-derived CD4$^+$ T cells from either WT (*pink*) or IL-5–deficient (*dark blue*) donor mice were transferred to TCR-α–deficient recipient mice to evaluate the role of IL-5–producing CD4$^+$ T cells in mediating the allergen-driven eosinophil-dominated type 2 protective response in allergy-free *Ascaris*-infected micd (**Δ**) (n = 5) and HDM-sensitized mice followed by *Ascaris* infection (HDM/A*scaris*) (**∇**) (n = 5) (**A**). Representative flow cytometry dot plot on lung tissue from TCR-α KO mice that received CD4$^+$ T cells from either WT (left) or IL-5 KO (right) donor mice (n = 5). Cells were stimulated with phorbol myristate acetate (PMA)/ionomycin (0.5/0.05 nM) and gated on live TCR-β$^+$CD4$^+$ T cells, showing the frequencies of IL-5 and IL-13 (**B**). Boolean analysis was performed to evaluate the frequency of polyfunctional T_H2 cells, including either IL-5$^+$IL-13$^-$IFN-γ$^-$IL-17A$^-$ (**C**) or IL-5$^+$IL-13$^+$IFN-γ$^-$IL-17A$^-$ (**D**) or finally IL-5$^-$IL-13$^+$IFN-γ$^-$IL-17A$^-$–producing CD4$^+$ T cells. Number of *Ascaris* larvae in the lungs on day 8 after infection (**F**), as well as lung-stage larval development by morphometric analysis of larvae recovered in the lungs from *Ascaris*-infected and HDM-sensitized/*Ascaris*-infected (HDM/*Ascaris*) mice in the presence or absence of IL-5–producing CD4$^+$ T cells (**G**). Representative bright confocal image of the larvae recovered in the bronchoalveolar lavage fluid on day 8 of infection of HDM/*Ascaris* mice that received WT CD4$^+$ T cells and HDM/*Ascaris* mice that received IL-5 KO CD4$^+$ T cells (scale 200 μm). The frequencies of Siglec–positive CD11c$^-$ eosinophils on day 8 after infection in the different groups (**H**). Each symbol represents a single mouse, and horizontal bars are geometric means. *P* values are indicated on each graph. Two independent experiments were performed. Differences between groups were considered statistically significant at *P* values less than .05 according to the Kruskal-Wallis test followed by the Dunn multiple comparison test.

(Fig 6, *C*) or IL-5$^+$IL-13$^+$ T_H2 effector cells (Fig 6, *D*), but also the differentiation of IL-5$^-$IL-13$^+$–producing T_H2 cells (0.5 ± 0.2 % vs 0.1 ± 0.1% [$P = .0317$] [Fig 6, *E*]). These data suggest that IL-5–producing CD4$^+$ T cells play a central role in establishing effector T_H2 cell–derived pulmonary inflammation.

Mice that received naive CD4$^+$ T cells capable of producing IL-5 exhibited reduced numbers of *Ascaris* parasites (223.0 ± 45.3 larvae vs 47.0 ± 20.3 larvae [$P < .0001$] [Fig 6, *F*]) and demonstrated arrested *Ascaris* larval development, as measured by larval size (59,339 ± 10,972 μm^2 vs 26,413 ± 8,580 μm^2

[$P < .0001$] [Fig 6, *G*]) following HDM sensitization. In contrast, mice that received $CD4^+$ T cells incapable of making IL-5 showed a significant reduction in lung eosinophils (33.1 ± 3.7 % vs 11.2 ± 3.61% [$P < .0500$]) (Fig 6, *H*), to a degree that allowed for normal *Ascaris* larval numbers (187.6 ± 54.84 larvae vs 240.8 ± 64.8 larvae [$P > .05$]) and development (69,704 ± 10,078 μm^2 vs 73,056 ± 10,466 μm^2 [$P > .05$]) (Fig 6, *F* and *G*). Together, these results suggest a critical role for IL-5–producing $CD4^+$ T cells in the IL-13–mediated eosinophil-dependent helminth larval killing.

DISCUSSION

HDMs are the most prevalent environmental allergens associated with pulmonary and airway allergic inflammation around the world,[25] whereas *Ascaris* is the most prevalent human helminth parasite worldwide.[1] The *Ascaris* life cycle in humans involves transient larval migration through lung tissue and airways that can lead to eosinophil-rich lung tissue inflammation, known as Löeffler syndrome,[26,27] a process similar to that seen in pulmonary allergic disorders. A common feature between both tissue-invasive helminth parasites and major environmental aeroallergens is their ability to induce strong type 2 inflammation (reviewed in Henry et al[28] and Santiago et al[29]), through a coordinated orchestration of innate (IL-33–, group 2 ILC–, and IL-4–derived eosinophils and epithelium hyperplasia),[30-32] adaptive (differentiation of IL-5– and IL-13–producing T_H2 effector cells,[33,34] and humoral (IgE and IgG4 class switching)[5,35] responses.

The immunologic interaction between these two type 2 inducers have allowed for a better understanding of both allergic inflammation[18] and protective responses against tissue-trafficking helminth parasites.[17] We have previously demonstrated that sensitization resulting from HDM allergy coincident with filarial infection in humans induces an expansion of parasite-specific polyfunctional T_H2 cells, with subsequent increases in secreted levels of IL-4, IL-5, and IL-13. In experimental models, it has also been shown that intranasal sensitization with HDM drives a $CD4^+$ T-cell–dependent lung-specific, eosinophil-rich type 2-immune response.[17]

However, how the cross talk between allergen-driven T_H effector cells and the subsequent eosinophil-dominated type 2 inflammation mediate host resistance against tissue-trafficking helminth parasites was not clear. To this end, we have demonstrated here that HDM allergen-mediated pulmonary inflammation relies on both IL-5– and on IL-13–producing T_H2 effector cells elicited by allergic sensitization. Our findings challenge the primacy of IL-5 being the only cytokine driving eosinophil differentiation, activation, survival, and recruitment to the site of inflammation.

Hogan et al[36] demonstrated that the transfer of primed ovalbumin (OVA)-specific $CD4^+$ T_H2 cells from OVA-sensitized WT mice into OVA-sensitized IL-$5^{-/-}$ mice was sufficient to restore blood and airway eosinophil numbers, lung damage, and airway hyperresponsiveness after antigen challenge. These data helped support the hypothesis that antigen-specific IL-5–secreting T_H2 cells played a central role in eosinophil recruitment and activation. Moreover, anti–IL-5 mAb administered before allergen challenge was shown to suppress eosinophil recruitment to the peripheral blood and airways in mouse models,[37] as well as helping to improve asthma clinical symptoms[38,39] and other certain forms of hypereosinophilic syndromes in humans.[40] Despite these data, the role played by IL-5 in mediating host resistance against tissue-trafficking helminth parasites is unclear. We have previously shown that HDM allergic sensitization in the lungs drives a $CD4^+$ T-cell–dependent eosinophil-rich type 2 immune response that arrests *Ascaris* larval development and limits parasite burden.[17] Nevertheless, in this present study, we have shown that *Ascaris* parasites are abundant and develop normally in lungs with HDM allergy in the absence of IL-5–producing T_H2 cell–derived eosinophils (Fig 6, *F* and *G*).

Because IL-5–producing $CD4^+$ T_H2 cells are also a major source of IL-13 in lungs with HDM allergy, we explored the role of IL-13 signaling in the lung tissue. We observed that in HDM-sensitized IL-13Rα1–deficient mice there was a dramatic suppression in CCL-11 (eotaxin-1) and CCL-24 (eotaxin-2) production that resulted in a significant reduction in the frequency of lung tissue eosinophils in the absence of IL-13 signaling (Fig 4). IL-13 is a pleiotropic cytokine that signals through the IL-13Rα1/IL-4Rα heterodimer to induce type 2–associated responses.[41] Because the receptors for IL-13 and IL-4 both contain IL-4Rα and signal through STAT6, it has been suggested that IL-4 and IL-13 might serve redundant functions.[42] However, helminth experimental models using IL-4–deficient and IL-13–deficient mice have revealed nonoverlapping functions of both cytokines.[43,44] For instance, after *Nippostrongylus brasiliensis* infection, WT and IL-4-deficient mice cleared worms whereas worm clearance in IL-13–deficient mice was significantly impaired,[45] a finding that is paralleled in the present study, in which inflammation due to HDM allergy in the absence of IL-13 signaling (IL13Rα$1^{-/-}$ mice) failed to control *Ascaris* larval numbers in the lungs and, conversely, was associated with lower parasite burden in IL-13Rα2–deficient mice (in which the bioactivity of IL-13 is considerably increased). Notably, the capacity of IL-13 to promote eosinophil accumulation in the lung and induce mucus hypersecretion (independently of IL-4 and/or IL-5) has been reported.[46-49]

Taken together, our data indicate that IL-5 is required for the induction of a polyfunctional allergen specific T_H2 effector cell response and that the subsequent signaling through the IL-13/IL13Ra1 axis in the lungs appears to be the major regulator of the number of eosinophils in the pulmonary tissue, which occurs through the induction of eotaxin-1 and eotaxin-2 (CCL-11 and CCL-24), with multiple bystander downstream consequences, including control of lung transiting parasitic helminths.

DISCLOSURE STATEMENT

Supported by the Division of Intramural Research, the National Institute of Allergy and Infectious Diseases (NIAID), NIH.

Disclosure of potential conflict of interest: The authors declare that they have no relevant conflicts of interest.

We are grateful to Professor Ricardo Fujiwara from the Federal University of Minas Gerais, Brazil and Dr Jianbin Wang from the University of Tennessee for providing the *Ascaris suum* eggs for the study. We are also thankful to Dr Justin Lack from the NIAID Collaborative Bioinformatics Resource, National Institutes of Health, for his insights on the single-cell RNA sequencing data.

Inclusion and diversity: We support inclusive, diverse, and equitable conduct of research.

REFERENCES

1. Gazzinelli-Guimaraes PH, Nutman TB. Helminth parasites and immune regulation. F1000Res 2018;7:F1000, Faculty Rev-1685.

2. Tuzlak S, Dejean AS, Iannacone M, Quintana FJ, Waisman A, Ginhoux F, et al. Repositioning TH cell polarization from single cytokines to complex help. Nat Immunol 2021;22:1210-7.
3. Kopf M, Le Gros G, Coyle AJ, Kosco-Vilbois M, Brombacher F. Immune responses of IL-4, IL-5, IL-6 deficient mice. Immunol Rev 1995;148:45-69.
4. Lebman DA, Coffman RL. Interleukin 4 causes isotype switching to IgE in T cell-stimulated clonal B cell cultures. J Exp Med 1988;168:853-62.
5. King CL, Nutman TB. IgE and IgG subclass regulation by IL-4 and IFN-gamma in human helminth infections. Assessment by B cell precursor frequencies. J Immunol 1993;151:458-65.
6. Strandmark J, Steinfelder S, Berek C, Kuhl AA, Rausch S, Hartmann S. Eosinophils are required to suppress Th2 responses in Peyer's patches during intestinal infection by nematodes. Mucosal Immunol 2017;10:661-72.
7. Klion AD, Nutman TB. The role of eosinophils in host defense against helminth parasites. J Allergy Clin Immunol 2004;113:30-7.
8. Klion AD, Ogbogu PU. Eosinophil-associated disorders. Preface. Immunol Allergy Clin North Am 2015;35:xi-xii.
9. Valent P, Klion AD, Rosenwasser LJ, Arock M, Bochner BS, Butterfield JH, et al. ICON: eosinophil disorders. World Allergy Organ J 2012;5:174-81.
10. Valent P, Gleich GJ, Reiter A, Roufosse F, Weller PF, Hellmann A, et al. Pathogenesis and classification of eosinophil disorders: a review of recent developments in the field. Expert Rev Hematol 2012;5:157-76.
11. Nagase H, Ueki S, Fujieda S. The roles of IL-5 and anti-IL-5 treatment in eosinophilic diseases: asthma, eosinophilic granulomatosis with polyangiitis, and eosinophilic chronic rhinosinusitis. Allergol Int 2020;69:178-86.
12. Doran E, Cai F, Holweg CTJ, Wong K, Brumm J, Arron JR. Interleukin-13 in asthma and other eosinophilic disorders. Front Med (Lausanne) 2017;4:139.
13. Bitton A, Avlas S, Reichman H, Itan M, Karo-Atar D, Azouz NP, et al. A key role for IL-13 signaling via the type 2 IL-4 receptor in experimental atopic dermatitis. Sci Immunol 2020;5:eaaw2938.
14. Wechsler ME, Klion AD, Paggiaro P, Nair P, Staumont-Salle D, Radwan A, et al. Effect of dupilumab on blood eosinophil counts in patients with asthma, chronic rhinosinusitis with nasal polyps, atopic dermatitis, or eosinophilic esophagitis. J Allergy Clin Immunol Pract 2022;10:2695-709.
15. Boes J, Eriksen L, Nansen P. Embryonation and infectivity of Ascaris suum eggs isolated from worms expelled by pigs treated with albendazole , pyrantel pamoate, ivermectin or piperazine dihydrochloride. Vet Parasitol 1998;75:181-90.
16. Gazzinelli-Guimaraes PH, Gazzinelli-Guimaraes AC, Silva FN, Mati VL, Dhom-Lemos Lde C, Barbosa FS, et al. Parasitological and immunological aspects of early Ascaris spp. infection in mice. Int J Parasitol 2013;43:697-706.
17. Gazzinelli-Guimaraes PH, de Queiroz Prado R, Ricciardi A, Bonne-Annee S, Sciurba J, Karmele EP, et al. Allergen presensitization drives an eosinophil-dependent arrest in lung-specific helminth development. J Clin Invest 2019;129:3686-701.
18. Gazzinelli-Guimaraes PH, Bennuru S, de Queiroz Prado R, Ricciardi A, Sciurba J, Kupritz J, et al. House dust mite sensitization drives cross-reactive immune responses to homologous helminth proteins. PLoS Pathog 2021;17:e1009337.
19. Karmele EP, Pasricha TS, Ramalingam TR, Thompson RW, Gieseck RL 3rd, Knilans KJ, et al. Anti-IL-13Ralpha2 therapy promotes recovery in a murine model of inflammatory bowel disease. Mucosal Immunol 2019;12:1174-86.
20. Zheng GX, Terry JM, Belgrader P, Ryvkin P, Bent ZW, Wilson R, et al. Massively parallel digital transcriptional profiling of single cells. Nat Commun 2017;8:14049.
21. Hao Y, Hao S, Andersen-Nissen E, Mauck WM 3rd, Zheng S, Butler A, et al. Integrated analysis of multimodal single-cell data. Cell 2021;184:3573-87.e29.
22. Aran D, Looney AP, Liu L, Wu E, Fong V, Hsu A, et al. Reference-based analysis of lung single-cell sequencing reveals a transitional profibrotic macrophage. Nat Immunol 2019;20:163-72.
23. Rose SA, Wroblewska A, Dhainaut M, Yoshida H, Shaffer JM, Bektesevic A, et al. A microRNA expression and regulatory element activity atlas of the mouse immune system. Nat Immunol 2021;22:914-27.
24. Zhu T, Brown AP, Cai LP, Quon G, Ji H. Single-cell RNA-seq analysis reveals lung epithelial cell type-specific responses to HDM and Regulation by Tet1. Genes (Basel) 2022;13:880.
25. Gregory LG, Lloyd CM. Orchestrating house dust mite-associated allergy in the lung. Trends Immunol 2011;32:402-11.
26. Chitkara RK, Krishna G. Parasitic pulmonary eosinophilia. Semin Respir Crit Care Med 2006;27:171-84.
27. Weatherhead JE, Gazzinelli-Guimaraes P, Knight JM, Fujiwara R, Hotez PJ, Bottazzi ME, et al. Host immunity and inflammation to pulmonary helminth infections. Front Immunol 2020;11:594520.
28. Henry EK, Inclan-Rico JM, Siracusa MC. Type 2 cytokine responses: regulating immunity to helminth parasites and allergic inflammation. Curr Pharmacol Rep 2017;3:346-59.
29. Santiago HC, Nutman TB. Human helminths and allergic disease: the hygiene hypothesis and beyond. Am J Trop Med Hyg 2016;95:746-53.
30. Tait Wojno ED, Artis D. Innate lymphoid cells: balancing immunity, inflammation, and tissue repair in the intestine. Cell Host Microbe 2012;12:445-57.
31. Wojno ED, Monticelli LA, Tran SV, Alenghat T, Osborne LC, Thome JJ, et al. The prostaglandin D(2) receptor CRTH2 regulates accumulation of group 2 innate lymphoid cells in the inflamed lung. Mucosal Immunol 2015;8:1313-23.
32. Johansson K, McSorley HJ. Interleukin-33 in the developing lung-roles in asthma and infection. Pediatr Allergy Immunol 2019;30:503-10.
33. de Ruiter K, Jochems SP, Tahapary DL, Stam KA, Konig M, van Unen V, et al. Helminth infections drive heterogeneity in human type 2 and regulatory cells. Sci Transl Med 2020;12:eaaw33703.
34. Gazzinelli-Guimaraes PH, Bonne-Annee S, Fujiwara RT, Santiago HC, Nutman TB. Allergic sensitization underlies hyperreactive antigen-specific CD4+ T cell responses in coincident filarial infection. J Immunol 2016;197:2772-9.
35. Turner JD, Faulkner H, Kamgno J, Kennedy MW, Behnke J, Boussinesq M, et al. Allergen-specific IgE and IgG4 are markers of resistance and susceptibility in a human intestinal nematode infection. Microbes Infect 2005;7:990-6.
36. Hogan SP, Koskinen A, Matthaei KI, Young IG, Foster PS. Interleukin-5-producing CD4+ T cells play a pivotal role in aeroallergen-induced eosinophilia, bronchial hyperreactivity, and lung damage in mice. Am J Respir Crit Care Med 1998;157:210-8.
37. Hogan SP, Koskinen A, Foster PS. Interleukin-5 and eosinophils induce airway damage and bronchial hyperreactivity during allergic airway inflammation in BALB/c mice. Immunol Cell Biol 1997;75:284-8.
38. Busse W, Chupp G, Nagase H, Albers FC, Doyle S, Shen Q, et al. Anti-IL-5 treatments in patients with severe asthma by blood eosinophil thresholds: Indirect treatment comparison. J Allergy Clin Immunol 2019;143:190-200.e20.
39. Flood-Page P, Swenson C, Faiferman I, Matthews J, Williams M, Brannick L, et al. A study to evaluate safety and efficacy of mepolizumab in patients with moderate persistent asthma. Am J Respir Crit Care Med 2007;176:1062-71.
40. Kim YJ, Prussin C, Martin B, Law MA, Haverty TP, Nutman TB, et al. Rebound eosinophilia after treatment of hypereosinophilic syndrome and eosinophilic gastroenteritis with monoclonal anti-IL-5 antibody SCH55700. J Allergy Clin Immunol 2004;114:1449-55.
41. Wynn TA. IL-13 effector functions. Annu Rev Immunol 2003;21:425-56.
42. Zurawski SM, Vega F Jr, Huyghe B, Zurawski G. Receptors for interleukin-13 and interleukin-4 are complex and share a novel component that functions in signal transduction. EMBO J 1993;12:2663-70.
43. McKenzie GJ, Bancroft A, Grencis RK, McKenzie AN. A distinct role for interleukin-13 in Th2-cell-mediated immune responses. Curr Biol 1998;8:339-42.
44. Bao K, Reinhardt RL. The differential expression of IL-4 and IL-13 and its impact on type-2 immunity. Cytokine 2015;75:25-37.
45. Urban JF Jr, Noben-Trauth N, Donaldson DD, Madden KB, Morris SC, Collins M, et al. IL-13, IL-4Ralpha, and Stat6 are required for the expulsion of the gastrointestinal nematode parasite Nippostrongylus brasiliensis. Immunity 1998;8:255-64.
46. Grunig G, Warnock M, Wakil AE, Venkayya R, Brombacher F, Rennick DM, et al. Requirement for IL-13 independently of IL-4 in experimental asthma. Science 1998;282:2261-3.
47. Wills-Karp M, Luyimbazi J, Xu X, Schofield B, Neben TY, Karp CL, et al. Interleukin-13: central mediator of allergic asthma. Science 1998;282:2258-61.
48. Webb DC, McKenzie AN, Koskinen AM, Yang M, Mattes J, Foster PS. Integrated signals between IL-13, IL-4, and IL-5 regulate airways hyperreactivity. J Immunol 2000;165:108-13.
49. Hogan SP, Matthaei KI, Young JM, Koskinen A, Young IG, Foster PS. A novel T cell-regulated mechanism modulating allergen-induced airways hyperreactivity in BALB/c mice independently of IL-4 and IL-5. J Immunol 1998;161:1501-9.